Serra T, Capelli C, Toumpaniari R, Orris I, Leong J, Dalgarno K, Kalaskar D. Design and fabrication of 3D-printed anatomically shaped lumbar cage for intervertebral disc (IVD) degeneration treatment. *Biofabrication* 2016, 8(3), 035001.

Biofabrication

PAPER

Design and fabrication of 3D-printed anatomically shaped lumbar cage for intervertebral disc (IVD) degeneration treatment

T Serra[1], C Capelli[2], R Toumpaniari[3], I R Orriss[4], J J H Leong[1,5], K Dalgarno[3] and D M Kalaskar[1]

[1] Division of Surgery & Interventional Science, Royal Free Hospital Campus, UCL, NW3 2PF, UK
[2] Centre for cardiovascular imaging, Institute of Cardiovascular Science, University College London WC1N 1EH, UK
[3] School of Mechanical and Systems Engineering, Newcastle University, Newcastle NE1 7RU, UK
[4] Department of Comparative Biomedical Sciences, Royal Veterinary College, London NW1 0TU, UK
[5] Royal National Orthopaedic Hospital NHS Trust, Stanmore HA7 4LP, UK

E-mail: d.kalaskar@ucl.ac.uk

OPEN ACCESS

RECEIVED
19 November 2015

REVISED
10 March 2016

ACCEPTED FOR PUBLICATION
9 June 2016

PUBLISHED
18 July 2016

Keywords: 3D printing, lumber cage, IVD, nano hydroxyapatide, finite element analysis, fabrication, design

Abstract

Spinal fusion is the gold standard surgical procedure for degenerative spinal conditions when conservative therapies have been unsuccessful in rehabilitation of patients. Novel strategies are required to improve biocompatibility and osseointegration of traditionally used materials for lumbar cages. Furthermore, new design and technologies are needed to bridge the gap due to the shortage of optimal implant sizes to fill the intervertebral disc defect. Within this context, additive manufacturing technology presents an excellent opportunity to fabricate ergonomic shape medical implants. The goal of this study is to design and manufacture a 3D-printed lumbar cage for lumbar interbody fusion. Optimisations of the proposed implant design and its printing parameters were achieved via *in silico* analysis. The final construct was characterised via scanning electron microscopy, contact angle, x-ray micro computed tomography (μCT), atomic force microscopy, and compressive test. Preliminary *in vitro* cell culture tests such as morphological assessment and metabolic activities were performed to access biocompatibility of 3D-printed constructs. Results of *in silico* analysis provided a useful platform to test preliminary cage design and to find an optimal value of filling density for 3D printing process. Surface characterisation confirmed a uniform coating of nHAp with nanoscale topography. Mechanical evaluation showed mechanical properties of final cage design similar to that of trabecular bone. Preliminary cell culture results showed promising results in terms of cell growth and activity confirming biocompatibility of constructs. Thus for the first time, design optimisation based on computational and experimental analysis combined with the 3D-printing technique for intervertebral fusion cage has been reported in a single study. 3D-printing is a promising technique for medical applications and this study paves the way for future development of customised implants in spinal surgical applications.

1. Introduction

Low back pain (LBP) is a very common musculoskeletal pathology in industrialised countries that affect around 80 per cent of adults during their lifetime [1, 2] and it is considered one of the most critical health problems, due to health and social costs associated with this condition. Severe LBP has been related to intervertebral disc degeneration (IVD) [2]. Surgical procedures such as lumbar fusion [3] or total disc replacement [4] are currently used for the treatment of chronic LBP when conservative therapies have been unsuccessful in rehabilitation of patients. In particular, fusion, the gold standard surgical procedure for both lumbar and cervical disease, often implies the use of an inter-body cage packed with bone graft to promote bone growth and fusion with the vertebrae.

Nowadays, the most commonly used cages in lumbar fusion treatment are made of titanium. They show good radiographic fusion rates and improved clinical results [5]. However, conventional titanium cages can present excessive stiffness, which might lead to adjacent level disorder, failure to promote bone growth and remodelling [6]. Furthermore, these cages are

crucially difficult to be visualised during follow-up imaging [7].

Alternative to titanium cages, polyether ether ketone (PEEK) cages have been increasingly used [8]. They provide similar stability to metallic cages and decrease the stress on the vertebral endplates owing to a modulus of elasticity closer to cortical bone [9]. However, new strategies in order to improve the biocompatibility and osseointegration of PEEK cages are strongly required in order to increase the fusion rate [8].

In addition, both titanium and PEEK cages are currently produced only in a limited number of standard sizes and shapes. Surgeons currently limit their choices to the availability of implant sizes and, in particular, the closest match to fill the defect from the excised IVD. Implant size mismatch can cause damage to the end plates on insertion. Undersized implants can lead to subsidence, and oversize implants can cause injuries to the neural structures. Importantly, the selection of an oversize cage can increase the risk of implant subsidence or failure. This was emphasised by Palissery and colleagues who highlighted the importance of avoiding implants size mismatch to stimulate regular bone integration [10]. The development of a novel anatomically shaped and potentially perfectly matched implants could lead to higher load transfer, preventing damage to cortical bone, and therefore accelerating the fusion process [11–13]. Potentially, such newly designed spinal cages will also allow a faster and more efficient planning of the surgical operation, and will reduce the risk of failure of the implant by ensuring improved matching with the patient vertebrae dimension and morphology (i.e. angles between endplates, shape and size).

Importantly, the manufacturing of such ergonomic/organic shape is now potentially achievable at low-cost by techniques such as additive manufacturing (AM). AM, commonly known as 3D-printing, has represented a breakthrough in the world of medical devices manufacturing. The capacity of this technique to fabricate customised 3D structures with complex geometries and excellent reproducibility has a potential to revolutionise implantology and regenerative medicine [14, 15].

In this context, the goal of this study is to design, develop and manufacture an anatomical 3D-printed lumbar cage based on a novel composite biomaterial for lumbar interbody fusion.

2. Materials and methods

The process of fabrication and testing of a novel, anatomically shaped, cage was divided into three stages: first, optimisation of cage design and 3D-manufacturing process; second, morphological–structural analysis and mechanical characterisation of the developed cage; and, third, *in vitro* biological evaluation.

2.1. Biomaterials

A proprietary nano-composite polymer, polyhedral oligomeric silsesquioxane poly (carbonate-urea) urethane (POSS-PCU) for medical applications previously developed by our group has been used in this study [16]. Its ability of functioning as a component of artificial organs [16], coatings for nanoparticles [17], and a platform that could be functionalized with bioactive molecules [18] have been proved. It has been used in three different first-in-man clinical studies as a lacrimal duct [16], as a bypass graft [19], and as the world's first synthetic trachea [20]. Polycarbonate (PC) is one of the engineering thermoplastic materials most commonly used and most widely tested in the medical device field [21]. PC filament (diameter = 1.75 mm, density = 1.20 gr cm^{-3}, and tensile modulus of 2350 MPa) has been used for fused deposition modelling (FDM) technology. Nano-hydroxyapatite (nHAp) (donated by Ceramisys Ltd, UK) has been used for the coating of the cage for its very well known capacity to promote osteo-integration of the implant.

2.2. Lumbar cage design and manufacturing

2.2.1. Design and optimisation via FEA

The geometry here proposed (figure 1) includes a curved profile, which resembles the contour of the vertebrae. The design was conceived for an anterior approach of interbody fusion. The new geometry aims to avoid uneven load transfer and fusion. Dimensions of cage design are based on average spacing between two adjacent vertebrate of adult lumbar region. Two cavities, representing 36% of the entire volume, are included with the purpose to support the bone tissue growth for fusion process to occur. Filling density is a fundamental parameter in the printing process. It specifies how hollow or solid the internal structure will be. A higher filling density gives a lower internal porosity and increases the amount of material and time consumption to fabricate the cage. As indicated in figures 1(d)–(g), four different filling densities were hypothesised with varying percentage of PC filling: 25%, 50%, 75%, and 100%.

Preliminary mechanical analyses were performed by means of finite element analyses (FEA) for the evaluation of polymer cage architectures and the influence of the different filling densities. PC was modelled as elastic material with Young's modulus = 2350 MPa and Poisson ratio = 0.3. The modelling of the different filling densities was translated by assigning different material properties to the core of the cage. Such different property was described by elastic material with 25%, 50%, and 75% of the PC Young's modulus [22]. The FEA were performed on two subsequent steps: first, a preliminary pressure of 2.5 MPa was applied;

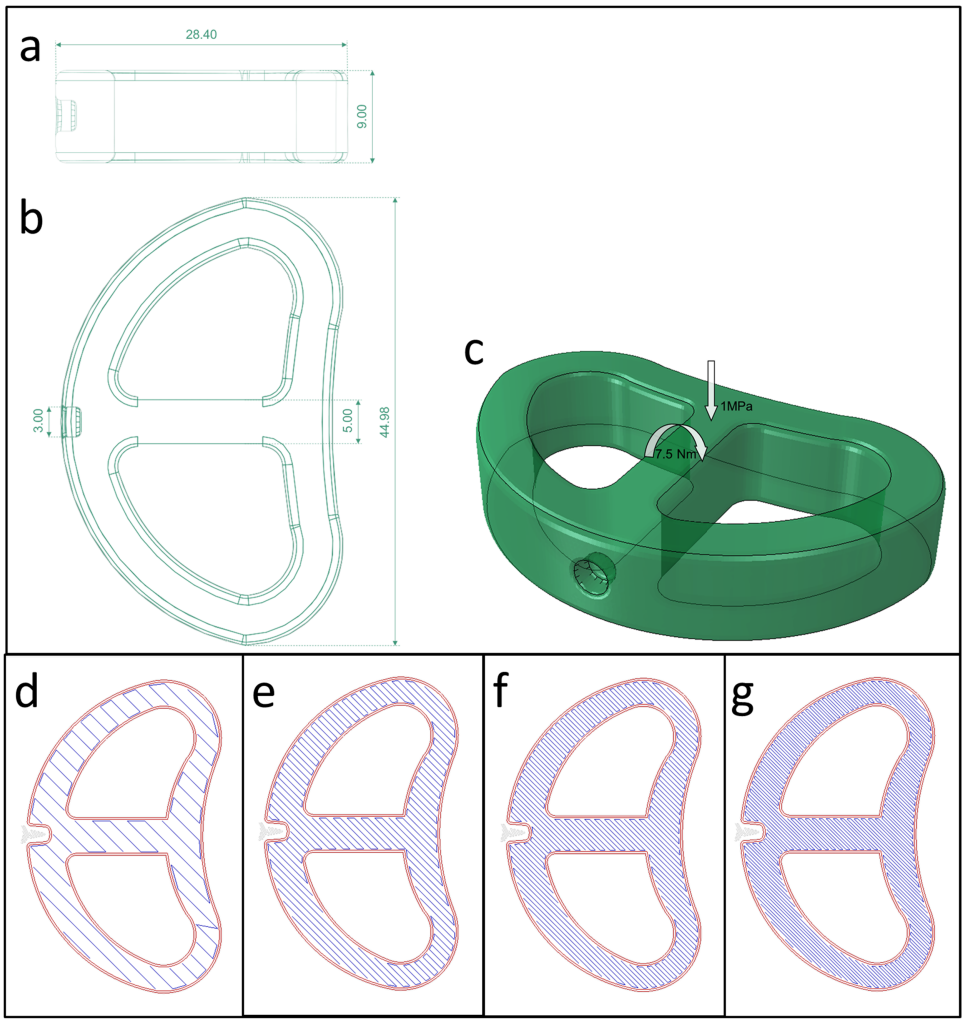

Figure 1. Design of the proposed lumbar cage: (a) lateral; (b) top and (c) prospective view. In addition the white arrows indicate the loads simulated on the device in FEA. Schematic of the four different filling densities hypothesised: (d) 25%, (e) 50%, (f) 75%, and (g) 100%.

corresponding to 1000 N distributed on the top surface of the cage; second, a moment of 15 Nm was imposed to the centre of mass of the device to simulate the bending forces. The magnitudes of the loads were chosen in accordance with numerical studies on the loads of lumbar segments of the spine [23]. Resulting stresses and strains were extracted and compared with the limits of failure for PC (i.e. 70 MPa) [24].

Table 1. Printing parameters.

Tn	265 °C
Nozzle diameter	0.3 mm
Print speed	10 mm s^{-1}
Layer height	0.2 mm
Ns	3
Filling density	25%
Tb	125 °C

2.2.2. Manufacturing optimisation

2.2.2.1. Printing parameters setup

For the manufacturing process, a FDM printer (Flashforge Dreamer, US) was used to fabricate the 3D structure with a layer-by-layer deposition of polymer. Following the optimisation, the parameters for the printing equipment were selected, such as temperature of the heating nozzle (Tn), nozzle diameter (Dn), print speed, layer height, number of external shells (Ns), filling density and temperature of the heated bed (Tb), shown in table 1. The previously developed CAD model was converted in .STL file and sliced to get 2D layers by using Slic3r software.

2.2.2.2. Coating

In order to improve biocompatibility and bioactivity of the printed polycarbonate cage, a two-steps coating procedure by using POSS-PCU and nHAp powder was carried out. Polymeric and nano-composite solutions were prepared for this purpose. Polymeric coating was composed by POSS-PCU dissolved in dimethylacetamide (DMAc) (20%w/w). Composite coating was obtained by mixing previously prepared

solution with nHAp powder (50:50 w/w) on an orbital mixer during 3 h in order to get a homogeneously dispersed slurry mixture. Polycarbonate cages were first immersed for 5 min in the polymeric solution then left to dry in oven at $T = 65\ ^{\circ}C$. A second 5 min immersion of the samples in the composite slurry was followed by solvent casting process at room temperature in order to avoid presence of cracks on the surface of the cage with a slow drying process.

2.3. Morphological analysis

A morphological evaluation of the nano-composite coating by scanning electron microscopy (SEM, Zeiss EVO HD15) was carried out. Previously, samples were sputter-coated with gold in an ion coater (Q150R, Quorum Technologies). Surface morphology of the POSS-PCU polymer as well as nHAp particles distribution was observed.

2.4. Wettability

Contact angle measurements were performed to evaluate the materials wettability. The sessile drop method was used to measure the contact angle by depositing ultrapure water (3 μl; Milli-Q; Millipore, USA) on the surfaces of the polymeric films using a contact angle measurement system (Kruss, DSA 100, Germany). Polymeric films were used to perform the measurements. Three samples of each material (POSS-PCU, POSS-PCU + nHAp) with the following dimensions: length = 3 cm, width = 1 cm, thickness = 0.1 cm, were used for the study. Three measurements were performed in each specimen, and independent experiments were conducted on three different samples.

2.5. Mechanical evaluation

Three cubic microstructures ($10 \times 10 \times 10\ mm^3$) reproducing the same microstructure and pattern organisation were tested. Samples were directly printed by previously designed CAD files. The real accurate dimensions of the specimens were measured before the test. A universal Testing Machine (Tinius Olsen, H25K-S UTM, USA) with a 2.5 KN load cell was used to evaluate the mechanical properties of the 3D polycarbonate PC structures. The samples were tested at a speed of $1\ mm\ min^{-1}$ without preloading. Stress–strain data were computed from load–displacement measurements. The compressive modulus was determined based on the slope of the stress–strain curve in the elastic region. Moreover, the compressive strength at 40% deformation (σ40%) was reported.

2.6. Microstructure analysis by x-ray microcomputed tomography (μCT)

Three cages for each material composition (PC and PC + POSS-PCU/nHAp coating) were scanned using a Skyscan 1172 μCT scanner (Bruker μCT, Kontich, Belgium) instrument with a voxel size of $20 \times 20 \times 20\ \mu m^3$. The μCT scanner was set at 40Kv and 250 μA using a pixel size of 28.67 μm without filter.

The images were reconstructed using the Skyscan Nrecon software and analysed using the Skyscan CTAn programme to determine the porosity as well as the presence of nHAp coating on the surface.

2.7. Topographical evaluation at the nanoscale by atomic force microscopy (AFM)

Surface topography as well as nHAp distribution at the surface of the composite materials was observed by atomic force microscopy (AFM system, Bruker, Multimode 8, Belgium) a non-destructive technique that allows measurement of surface topography in 3D at the nanoscale. The studied parameters were: surface roughness (Sa), skewness, or the asymmetry of the surface about the mean plane (Ssk), and kurtosis, or peakedness of the surface about the mean plane (Sku). An ANOVA test was performed to determine the statistical significance ($p \leqslant 0.05$) of the differences in the values of compressive modulus and strength.

2.8. *In vitro* biological response

14 mm diameter films were seeded with 2×104 adipose derived stem cells (ADSCs) and tests of metabolic activity and morphology were carried out.

Metabolic activity after 1, 3, 7, 14, and 21 days of incubation was assessed with a resazurin assay (Alamar Blue, Life Technologies). Three replicates ($n = 3$) for each material were performed. All samples were cultured for 28 days in Low Glucose DMEM medium, 10% FBS, 1% penicillin/streptomycin.

In order to observe the morphology of the cells attached to the studied surfaces, fluorescence staining was performed. After 24 h of culturing, the cells were fixed by immersion in 4% paraformaldehyde in 10 mM phosphate buffered saline (PBS) at room temperature (RT) for 15 min. The cells were rinsed with a mixture of 10 mM PBS. Subsequently, the cells were permeablised with 0.1% Triton X-100 for 8 min at RT, washed three times in PBS. Tetramethylrhodamine conjugated rhodamine phalloidin (R415, Life Technologies Ltd, UK) diluted to a working concentration of 1:50 in 1%BSA was then added to the samples and left for 30 min. Nuclear staining using 4′,6-Diamidino-2-Phenylindole, Dihydrochloride (DAPI, Life Technologies Ltd, UK) dye was applied diluted in PBS with a ratio of 1:1000 having 300 nM staining solution for 4 min. The samples were then screened for stained cells using fluorescent microscope. Cell area and circularity were determined from fluorescence images after 24 h of culturing by using ImageJ software ($n = 50$ cells for each material).

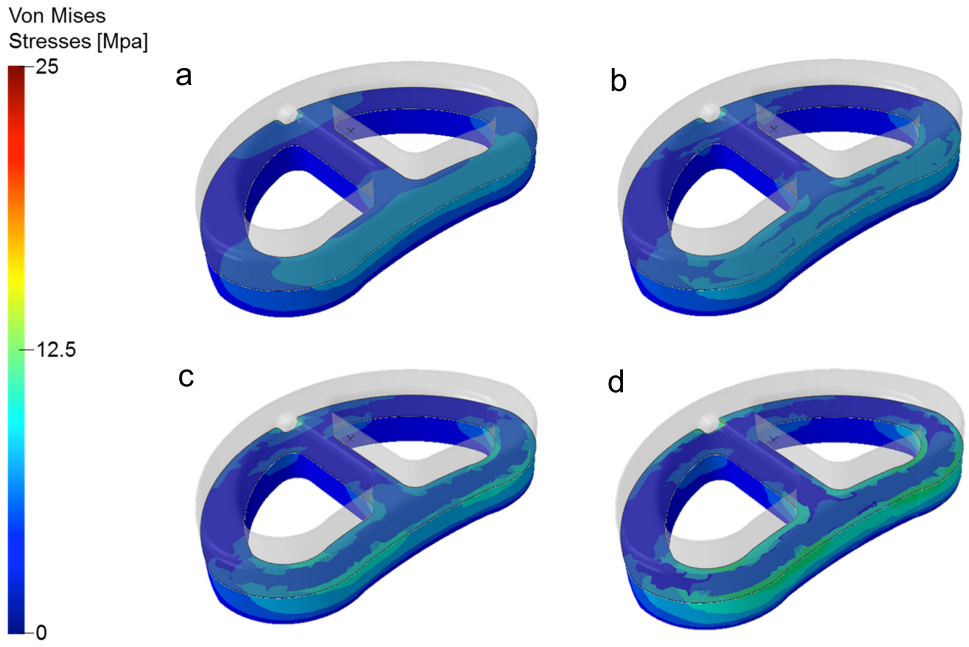

Figure 2. Von Mises stress distribution for the (cross-section) of four model of lumbar cage design with varying fillings: (a) 100%, (b) 75%, (c) 50% and (d) 25%. The scale is normalised to the maximum value of 25 MPa for visualising the differences of stress distribution.

3. Results

3.1. In silico analysis

Results of FEA of the proposed lumbar cage are reported in figure 2 at the moment of maximum load following the application of an axial bending moment. The distribution of Von Mises stresses varies according to the different percentage of filling density.

The peak of the stresses varies between 14.1 MPa for the 100% filling density and 34.1 MPa for the model of 25% filling density. In all the cases, there was no presence of abnormal high stress concentration that could lead to the implant failure. The stress distribution across the space show how the majority of loading support is provided by the outer wall. This is particularly evident for the two lowest density cases (figures 2(c) and (d)).

3.2. Morphological analysis by SEM

Figure 3(a) shows a prototype of the printed cage with and without POSS-PCU and nHAp coating. Figures 3(b)–(d) magnifies cross-sectional views of the polymeric (POSS-PCU) and composite (first layer of POSS-PCU, then a second along with nHAp). A homogeneous POSS-PCU/nHAp coating with a layer thickness around 100 μm is indicated by white arrows (figure 3(b)).

3.3. Contact angle evaluation

Contact angle values for the studied materials are reported in table 2. Overall, the presence of nHAp strongly decreased the contact angle values of the polymer blends in comparison to pure POSS-PCU.

3.4. Compressive test

Compressive modulus value was found to be 257.99 $\pm$ 6.69 MPa, value that is within the range of trabecular bone values (50–500 MPa) [25]. Compressive strength at 40% of deformation was 40.49 $\pm$ 2.37 MPa, up to 20 times higher than the values of the trabecular bone [25].

3.5. Microstructure characterisation by μCT

μCT images in figure 4 confirm the porosity of the model with 25% fill density. These observations were in accordance with previously selected parameters in the prototyping software. The POSS-PCU coating was homogeneously dispersed onto the cage surface, as highlighted in figure 4(c). Microstructure evaluation showed highly porous core 3D structure, with interconnectivity between pores.

3.6. Topographical evaluation by AFM

As described in table 3, average roughness (Sa) of POSS-PCU increased by including hydroxyapatite nanoparticles. Presence of bioactive nHAp particles added topographical cues to the composite surface conferring important biophysical signals for following biological studies. No statistically significant differences were found in term of surface asymmetry and peakedness by addition of nHAp particles. Figure 5 showed both 2D and 3D mapping of the surface for the polymeric POSS-PCU and the composite material containing nHAp particles.

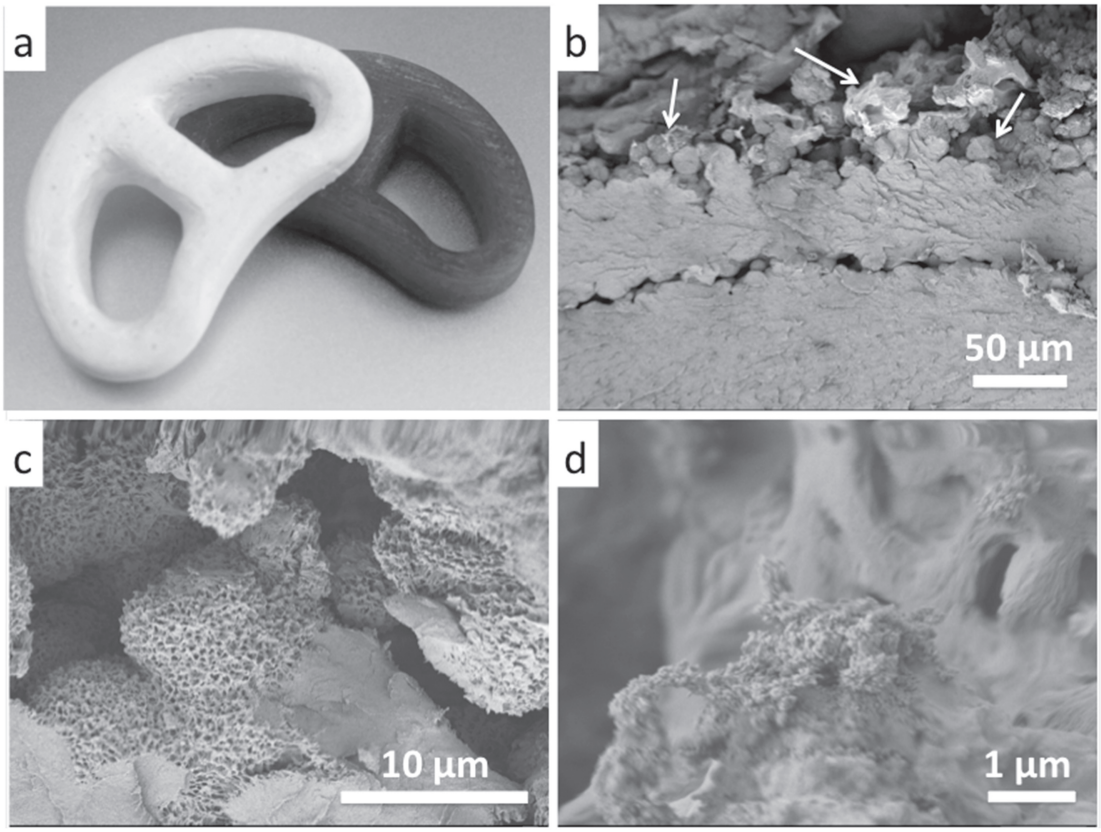

Figure 3. (a) A prototype fabricated with the patient specific design, with and without coating. SEM analysis of hydroxyapatite coating of polymer used for 3D-printing: (b) cross-sectional view of printing polymer coated with nano-composite material containing bioactive nano hydroxyapatite nHAp particles. White arrows show coating thickness and nHAp crystals exposed on the surface (c), (d) higher magnification of polymer surface coated with nHAp particles show topography at the micro and nanoscale.

Table 2. Contact angle evaluation for the polymeric and composite materials used (values ± SD).

Material	POSS-PCU	POSS-PCU + nHAp
Distilled and deionized water (°)	98.77 ± 0.72	11.56 ± 1.53

3.7. Cell assessment

Cytoskeleton staining using F-Actin was undertaken to evaluate the effect of surface modification on ADSCs. Cells cultured on all the test samples showed polygonal morphology (figure 6). Morphological evaluation at 24 h (figures 6(a)–(c)), showed stretched cytoskeleton for the cell seeded on all the set of materials. Figures 6(d) and (e) showed no statistically significant differences in term of cell circularity and area between POSS-PCU and the nHAp-coated one. Metabolic activity assay (figure 6(f)) showed similar number of viable cells at the early stage of seeding (day 1–3) for POSS-PCU and POSS-PCU + nHAp. Higher value was observed for the polymeric samples at day 7. Finally, the composite material presented higher metabolic activity at longer time of culturing (day 14–21).

4. Discussion

Novel approaches for scalable and flexible healthcare manufacturing solutions are strongly required by clinic and medical devices market [26]. In this perspective, the proposed work focused on assessing the suitability of a low-cost FDM system to fabricate an intervertebral fusion cage. In particular, 3D-printing technology was used to fabricate a nano-composite based on anatomically shaped lumbar cage. After a preliminary optimisation of the design via *in silico* analysis, cage's printing parameters were optimised and the achieved construct was physically characterised to ensure its compatibility for load bearing applications as spinal implant. In addition preliminary *in vitro* cell culture tests were performed to access biocompatibility of final constructs.

3D-printing process consists of highly complex procedure that combines hardware, software and material properties optimisation [27]. The selection of an optimal set of parameters allowed the generation of well-defined structure with smooth surface-finish. This is due to the deposition of the compact 3 layer external shell along with slow printing speed of 10 mm s^{-1} (as shown in table 1).

Main limitation factors to print suitable cages were the maximum temperature achieved with the heating

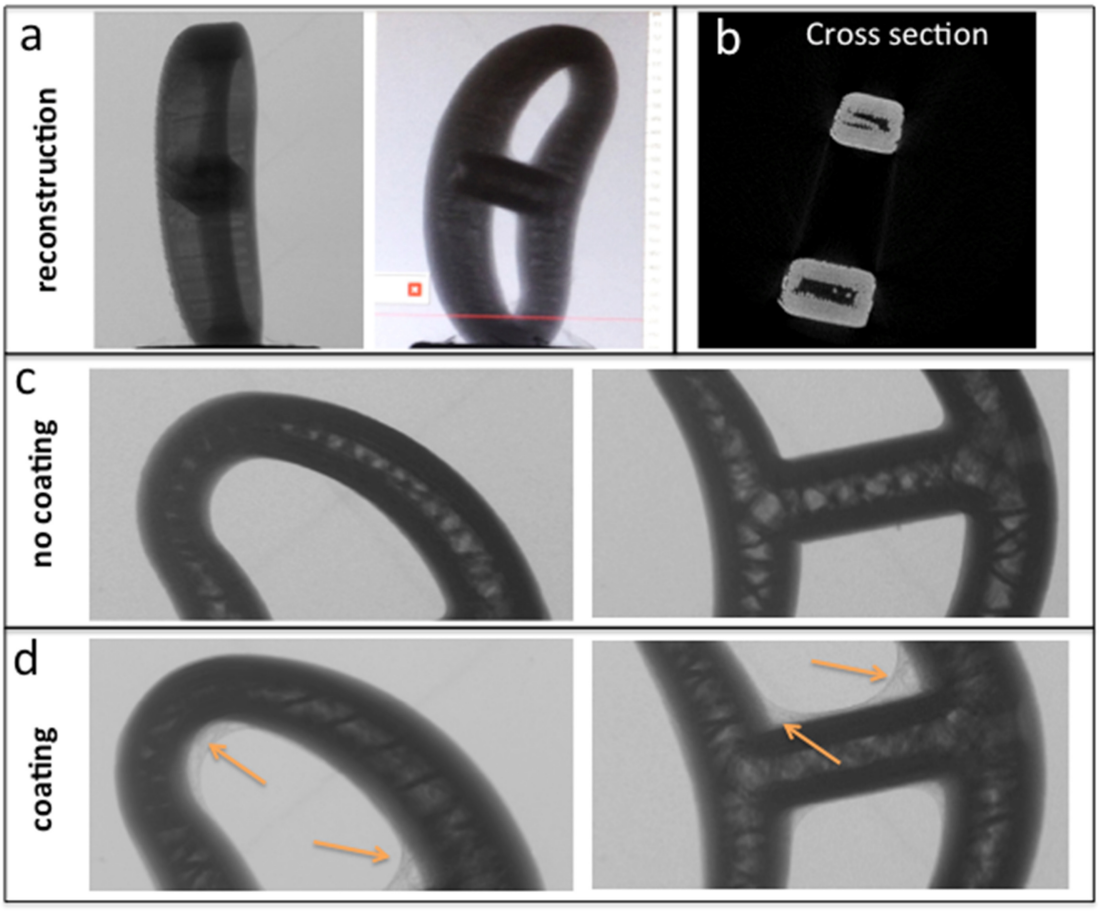

Figure 4. MicroCT images of the 3D-printed devices: (a) 3D view and (b) cross-section of the designed cage highlighting the internal porosity. 2D μCT slices for a no coated (c) and coated cage (d). Arrows show presence of POSS-PCU coating.

Table 3. Roughness parameters for the studied materials (values ± SD).

	POSS-PCU	POSS-PCU + nHAp
Sa (nm)	4.15 ± 0.16	10.2 ± 0.23
Ssk	0.413 ± 0.26	0.458 ± 0.11
Sku	4.03 ± 0.44	4.02 ± 0.06

nozzle (Tn = 265 °C) and heating bed (Tb = 125 °C) by the commercial printer used in this study. As PC filament requires higher melting temperature (275 °C–285 °C). This lack of higher temperatures for the material dispensing leads to detachment of the samples from the bed before the end of the process, at an expense of resolution and printing time. In order to remedy to this restriction and fix the optimal set of parameters, a faster process was adopted by decreasing the filling density from 100% to 25% of total volume for the core of the cage. In this scenario, FEA were used to verify the design and plan the manufacturing process. Therefore, careful consideration on the selection of lower filling density has been done as it clearly influences the mechanical properties of the final cage device. For instance, too low filling density, with consequent poor interconnection point among the printed layers, could lead to failure of implant during the application of mechanical loads. In the case of lumbar cage, it is of paramount importance to get adequate mechanical properties in order to support the human physiological loads. *In silico* analysis, showed in figure 2, was a useful method to preliminary test the cage design and to find an optimal value of filling density without compromising mechanical properties of the construct. An economic and faster method to manufacture 3D-printed cages with suitable mechanical properties by using a 25% of filling density was developed. The co-relation between designed and manufactured cage specimen was confirmed by the micro-CT evaluation, which confirmed highly porous and interconnected architecture similar to CAD design, confirming accuracy of the manufacturing process.

It is very well known that coating the surface of spinal inter-body implants with osteoconductive materials such as hydroxyapatite—can enhance osseointegration [10, 28]. In the case of PEEK devices coated with hydroxyapatite, the bone fusion process can be compromised due to the lack of physical bonding between PEEK and HAp [28, 29]. In our study, suitable hydroxyapatite coating of the lumbar cage was achieved by mixing nHAp with POSS-PCU polymer,

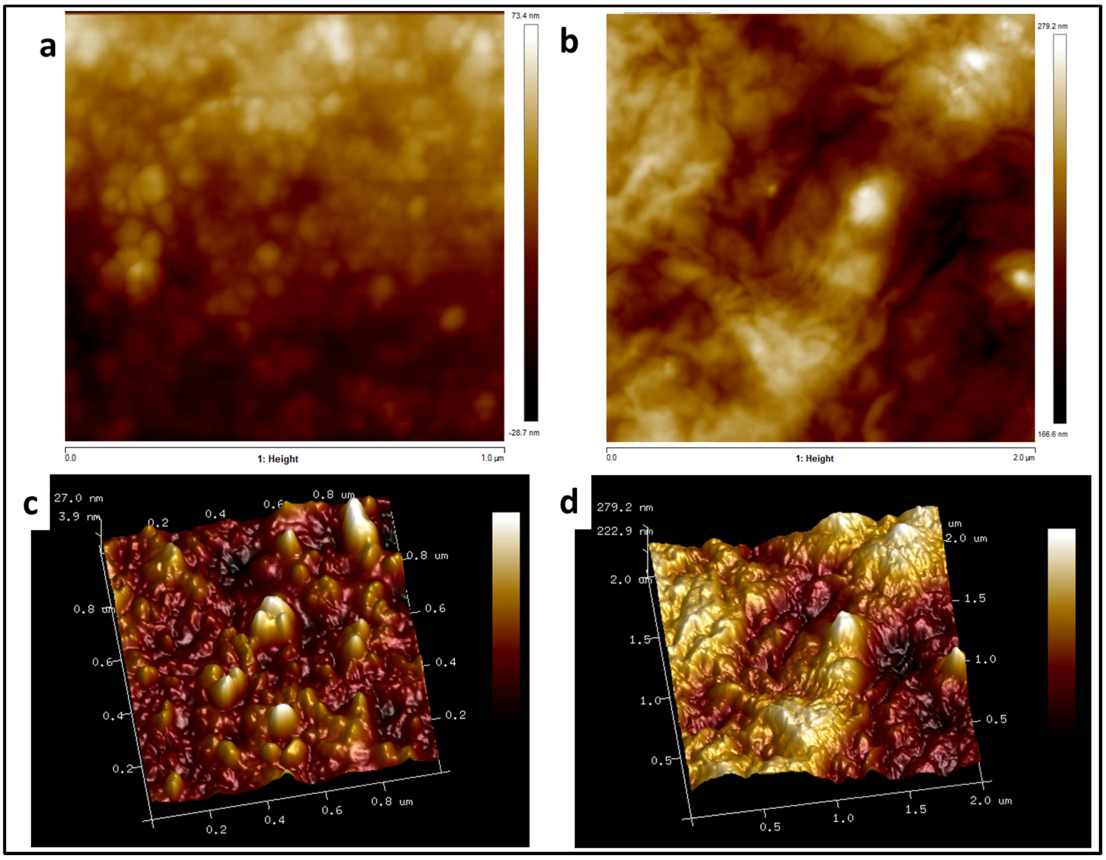

Figure 5. (a), (b) 2D and (c), (d) 3D mapping of the surface for polymeric (a), (c) and composite (b), (d) surface.

which integrates well with PC core of the cage ensuring optimal interface bonds. Morphological examination by SEM of the cage' surface coating showed homogeneously dispersed nHAp particles embedded in a biocompatible POSS-PCU polymer matrix. Also, the low cooling rate used during the casting procedure (at room temperature) was suitable to avoid presence of cracks on the surface of the cage. POSS-PCU acted as a suitable matrix in order to cover PC cages with a thin layer of biocompatible and bioactive material. In addition, nHAp particles agglomeration on the surface introduced an interesting topography at the micro and nano-scale. Nevertheless, investigation should be done to assess if the presence of biochemical and biophysical signals gained by the introduction of nHAp particles will influence stem cells differentiation.

When 3D-printed cages were mechanically tested for compressive modulus, the values similar to trabecular bone were obtained compared to values reported for commercial metallic and PEEK based cages reported in literature [25, 30]. Mechanical properties of implant close to surrounding bone are important as this has an impact on stress shielding and integration of implant for bone fusion. However, further mechanical tests which stimulate motion of spine are required to test this in future.

The effect of topographical cues (such as surface roughness, peaks or grooves) on cell behaviour has been widely studied [31–33]. Coating of 3D printed cage with nHAp lead to decrease in water contact angle, confirming presence of hydrophilic nHAp on the surface. This was further confirmed by AFM and SEM analysis. The average surface roughness (Sa) of the POSS-PCU coated cages increased from 4.15 $\pm$ 0.16 nm to 10.2 $\pm$ 0.23 nm following coating process.

To confirm manufactured cages using 3D printing process and coated with nHAp showed biocompatible characteristics, they were tested with ADSCs in preliminary sense. Cell behaviour was assessed for their morphology and growth using cytoskeleton staining and metabolic activity. In spite of changes in surface roughness, cells did not show any significant change in cell morphology. This was confirmed with average cell area and circularity measurements. Metabolic activity studies over period of 3 weeks showed cell growth all samples with higher activity on nHAp coated samples. This can be attributed to its biological functions. Further long term biological assessments will be required to access suitability of these nano-composite materials in promoting osteogenic differentiation and modulating the foreign body reaction towards tissue healing and remodelling, which will be important for fusion process in real life applications. In the future, more appropriate mechanical tests (i.e. fatigue tests in accordance with ASTM F2077) should be performed and accurate preclinical testing of this postulate in a large

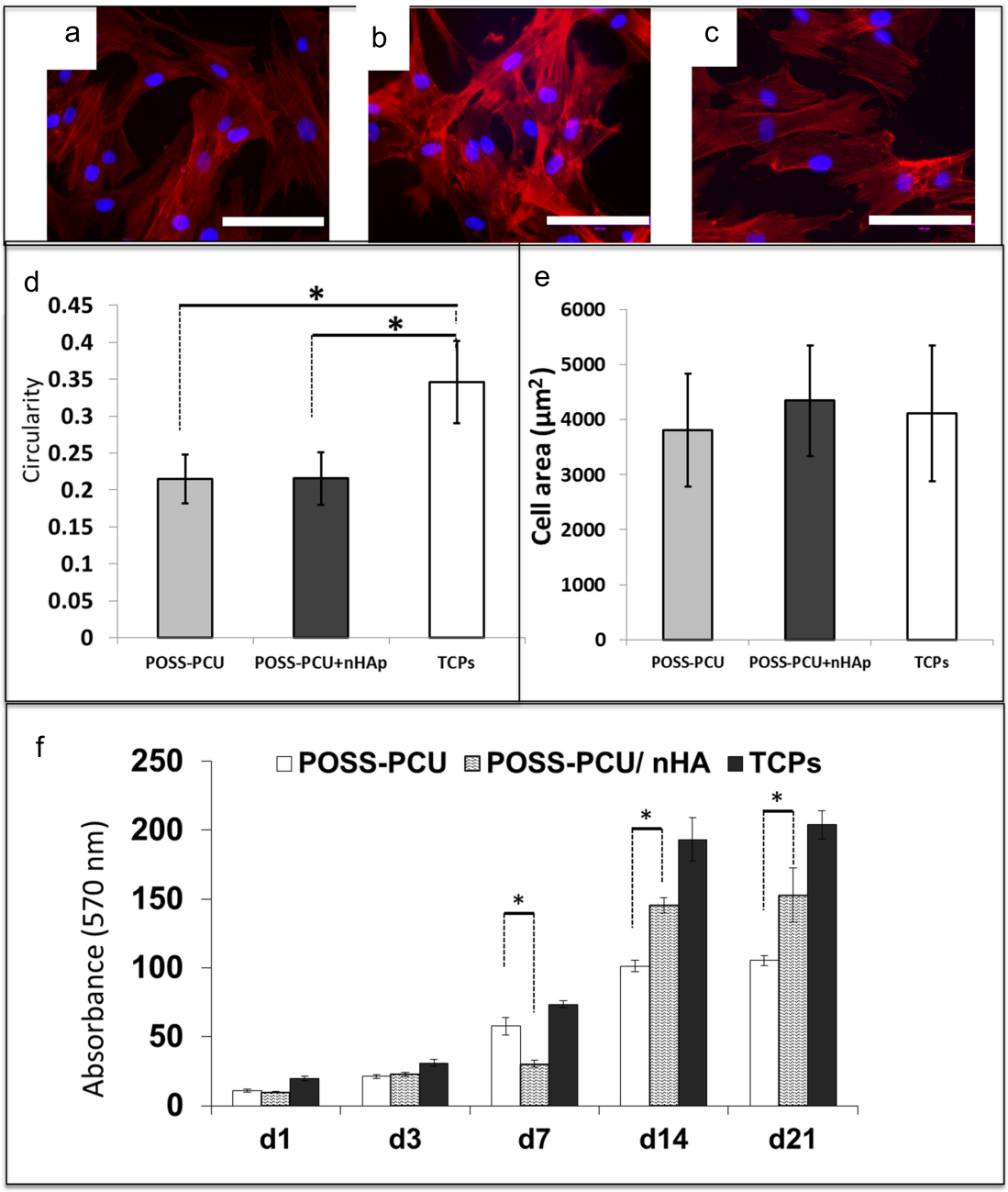

Figure 6. Fluorescence images of attached cells on (a) POSS-PCU, (b) POSS-PCU/nHAp and (c) TCPs at 24 h. Dapi in blue showed nuclei, phalloidin in red for actin cytoskeleton.(d) Cell circularity and (e) cell area evaluation by Image J software on $n = 50$ cells for each condition. (f) Metabolic activity calculated via Alamar Blue assay ($n = 3$). The values marked with an asterisk (*) showed statistical significant differences ($p \leqslant 0.05$).

animal model will be required. The work proposed is a feasibility study on the application of 3D printing for the manufacturing of healthcare solution exploring the potential impact of such technology to reduce costs of personalised implants.

5. Conclusion

In this study a novel method to develop anatomically shaped lumbar cage for fusion has been proposed. Design optimisation based on computational and experimental analysis combined with the 3D-printing technology provides a faster, scalable and inexpensive method to fabricate anatomically shaped cages for spinal fusion applications. This study paves the way for further exploration of 3D printing technology for customisable implants for various medical applications.

Acknowledgments

The authors thank UK-EPSRC Centre for Innovative Manufacturing of Medical Devices (MeDe Innovation, EPSRC grant EP/K029592/1) for financial support and Ceramisys Ltd for donating nano-hydroxyapatite.

References

[1] Burton A K *et al* 2006 European guidelines for prevention in low back pain *Eur. Spine J.* **15** (Suppl. 2) S136–68

[2] Malandrino A, Noailly J and Lacroix D 2011 The effect of sustained compression on oxygen metabolic transport in the intervertebral disc decreases with degenerative changes *PLoS Comput. Biol.* **7** e1002112

[3] Giorgi H, Prébet R, Delhaye M, Aurouer N, Mangione P, Blondel B, Tropiano P, Fuentes S and Parent H F 2015 French Society of Sprine Surgery (SFCR) Minimally invasive posterior transforaminal lumbar interbody fusion: One-year postoperative morbidity, clinical and radiological results of a prospective multicenter study of 182 cases *Orthop. Traumatol. Surg. Res.* **101(6 Suppl)** S241–5

[4] Thavaneswaran P and Vandepeer M 2014 Lumbar artificial intervertebral disc replacement: a systematic review *ANZ J. Surg.* **84** 121–7

[5] Kuslich S D, Ulstrom C L, Griffith S L, Ahern J W and Dowdle J D 1998 The Bagby and Kuslich method of lumbar interbody fusion, history, techniques, and 2-year follow-up results of a United States prospective, multicenter trial *Spine* (Phila Pa 1976) **23** 1267–78 ; discussion 1279

[6] Kanayama M, Cunningham B W, Haggerty C J, Abumi K, Kaneda K and McAfee P C 2000 In vitro biomechanical investigation of the stability and stress-shielding effect of lumbar interbody fusion devices *J Neurosurg.* **93** 259–65

[7] Cizek G R and Boyd L M 2000 Imaging pitfalls of interbody spinal implants *Spine* (Phila Pa 1976) **25** 2633–6

[8] Nemoto O, Asazuma T, Yato Y, Imabayashi H, Yasuoka H and Fujikawa A 2014 Comparison of fusion rates following transforaminal lumbar interbody fusion using polyetheretherketone cages or titanium cages with transpedicular instrumentation *Eur. Spine J.* **23** 2150–5

[9] Vadapalli S, Sairyo K, Goel V K, Robon M, Biyani A, Khandha A and Ebraheim N A 2006 Biomechanical rationale for using polyetheretherketone (PEEK) spacers for lumbar interbody fusion-A finite element study *Spine* (Phila Pa 1976) **31** E992–8

[10] Palissery V, Mulholland R C and McNally D S 2009 The implications of stress patterns in the vertebral body under axial support of an artificial implant *Med. Eng. Phys.* **31** 833–7

[11] Eswaran S K, Gupta A, Adams M F and Keaveny T M 2006 Cortical and trabecular load sharing in the human vertebral body *J. Bone Miner. Res.* **21** 307–14

[12] Fields A J, Lee G L and Keaveny T M 2010 Mechanisms of initial endplate failure in the human vertebral body *J. Biomech.* **43** 3126–31

[13] Smit T H, Müller R, van Dijk M and Wuisman P I 2003 Changes in bone architecture during spinal fusion: three years follow-up and the role of cage stiffness *Spine* **28** 1802–8 (discussion1809)

[14] Serra T, Mateos-Timoneda M A, Planell J A and Navarro M 2013 3D printed PLA-based scaffolds: a versatile tool in regenerative medicine *Organogenesis* **9** 239–44

[15] Melchels F P W, Domingos M A N, Klein T J, Malda J, Bartolo P J and Hutmacher D W 2012 Additive manufacturing of tissues and organs *Prog. Polym. Sci.* **37** 1079

[16] Chaloupka K, Motwani M and Seifalian A M 2011 Development of a new lacrimal drainage conduit using POSS nanocomposite *Biotechnol. Appl. Biochem.* **58** 363–70

[17] Tan A, Madani S Y, Rajadas J, Pastorin G and Seifalian A M 2012 Synergistic photothermal ablative effects of functionalizing carbon nanotubes with a POSS-PCU nanocomposite polymer *J. Nanobiotechnology* **10** 1–8

[18] de Mel A, Punshon G, Ramesh B, Sarkar S, Darbyshire A, Hamilton G and Seifalian A M 2009 In situ endothelialisation potential of a biofunctionalized nanocomposite biomaterial-based small diameter bypass graft *Biomed Mater Eng.* **19(4–5)** 317–31

[19] Ahmed M 2011 Design and development of a prosthetic implant for cardiovascular reconstructions Doctoral Thesis, UCL (University College London (http://discovery.ucl.ac.uk/1334080/)

[20] Jungebluth P *et al* 2011 Tracheobronchial transplantation with a stem-cell-seeded bioartificial nano-composite: a proof of-concept study *Lancet* **378** 1997–2004

[21] Lu F, Kang G, Jiang H, Zhang J and Liu Y 2014 Experimental studies on the uniaxial ratchetting of polycarbonate polymer at different temperatures *Polym. Test.* **39** 92–100

[22] Hellmich C, Fritsch A and Dormieux L 2011 Multiscale homogenization theory: an analysis tool for revealing mechanical design principles in bone and bone replacement materials *Biomimetics - Materials, Structures and Processes, Biological and Medical Physics, Biomedical Engineering* (Berlin: Springer) pp 81–103

[23] Noailly J, Lacroix D and Planell J A 2005 Finite element study of a novel intervertebral disc substitute *Spine* **30** 2257–64

[24] Williams J G 1984 *Fracture Mechanics of Polymers* (Chichester, UK: Ellis Horwood)

[25] Hench L L and Wilson J 1993 *An Introduction to Bioceramics* (Singapore: World Scientific) pp 25–40

[26] Mohanty S, Larsen L B, Trifol J, Szabo P, Burri H V, Canali C, Dufva M, Emnéus J and Wolff A 2015 Fabrication of scalable and structured tissue engineering scaffolds using water dissolvable sacrificial 3D printed moulds *Mater. Sci. Eng.* C **55** 569–78

[27] Zein D W, Hutmacher K C and Tan S H 2002 Teoh. Fused deposition modeling of novel scaffold architectures for tissue engineering applications *Biomaterials* **23** 1169–85

[28] Rao P J, Pelletier M H, Walsh W R and Mobbs R J 2014 Spine interbody implants: material selection and modification, functionalization and bioactivation of surfaces to improve osseointegration *Orthop. Surg.* **6** 81–9

[29] Zhao Y, Wong H M, Wang W, Li P, Xu Z, Chong E Y, Yan C H, Yeung K W and Chu P K 2013 Cytocompatibility, osseointegration, and bioactivity of three-dimensional porous and nanostructured network on polyetheretherketone. *Biomaterials* **34** 9264–77

[30] Kurtz S M and Devine J N 2007 PEEK biomaterials in trauma, orthopedic, and spinal implants *Biomaterials* **28** 4845–69

[31] Chen S, Jones J A, Xu Y, Low H Y, Anderson J M and Leong K W 2010 Characterization of topographical effects on macrophage behavior in a foreign body response model *Biomaterials* **31** 3479–91

[32] Deng Y, Liu X, Xu A, Wang L, Luo Z, Zheng Y, Deng F, Wei J, Tang Z and Wei S 2015 Effect of surface roughness on osteogenesis *in vitro* and osseointegration *in vivo* of carbon fiber-reinforced polyetheretherketone-nanohydroxyapatite composite *Int J Nanomedicine* **10** 1425–47

[33] Kunzler T P, Drobek T, Schuler M and Spencer N D 2007 Systematic study of osteoblast and fibroblast response to roughness by means of surface-morphology gradients *Biomaterials.* **28** 2175–82